# Three-dimensional quantitative structure-activity relationship (3 D-QSAR) and docking studies on (benzothiazole-2-yl) acetonitrile derivatives as c-Jun N-terminal kinase-3 (JNK3) i...

**ARTICLE** *in* BIOORGANIC & MEDICINAL CHEMISTRY LETTERS · DECEMBER 2006

Impact Factor: 2.42 · DOI: 10.1016/j.bmcl.2006.06.039 · Source: PubMed



**9 AUTHORS**, INCLUDING:

Abdul Rajjak Shaikh
Kobe University
**32** PUBLICATIONS **357** CITATIONS
SEE PROFILE

Mohamed Ismael
Sohag University
**39** PUBLICATIONS **562** CITATIONS
SEE PROFILE

Carlos A. Del Carpio
Kyoto Institute of Technology
**123** PUBLICATIONS **891** CITATIONS
SEE PROFILE

Ewa Broclawik
Polish Academy of Sciences
**154** PUBLICATIONS **1,451** CITATIONS
SEE PROFILE

Available online at www.sciencedirect.com
ScienceDirect
Bioorganic & Medicinal Chemistry Letters 16 (2006) 5917–5925
Bioorganic & Medicinal Chemistry Letters

# Three-dimensional quantitative structure–activity relationship (3 D-QSAR) and docking studies on (benzothiazole-2-yl) acetonitrile derivatives as c-Jun N-terminal kinase-3 (JNK3) inhibitors

Abdul Rajjak Shaikh,[a] Mohamed Ismael,[a] Carlos A. Del Carpio,[a,*] Hideyuki Tsuboi,[a] Michihisa Koyama,[a] Akira Endou,[a] Momoji Kubo,[a,b] Ewa Broclawik[c] and Akira Miyamoto[a,d,*]

[a]*Department of Applied Chemistry, Graduate School of Engineering, Tohoku University, 6-6-11-1302 Aoba, Aramaki, Aoba-ku, Sendai 980-8579, Japan*
[b]*PRESTO, Japan Science and Technology Agency, 4-1-8 Honcho, Kawaguchi, Saitama 332-0012, Japan*
[c]*Institute of Catalysis, Polish Academy of Sciences, ul. Niezapominajek 8, 30-239 Kraków, Poland*
[d]*New Industry Creation Hatchery Centre, Tohoku University, 6-6-10 Aoba, Aramaki, Aoba-ku, Sendai 980-8579, Japan*

Received 11 April 2006; revised 25 May 2006; accepted 13 June 2006
Available online 20 September 2006

**Abstract**—Three-dimensional quantitative structure–activity relationship (3D-QSAR) models were developed for 44 (benzothiazole-2-yl) acetonitrile derivatives, inhibiting c-Jun N-terminal kinase-3 (JNK3). It includes molecular field analysis (MFA) and receptor surface analysis (RSA). The QSAR model was developed using 34 compounds and its predictive ability was assessed using a test set of 10 compounds. The predictive 3D-QSAR models have conventional $r^2$ values of 0.849 and 0.766 for MFA and RSA, respectively; while the cross-validated coefficient $r^2_{cv}$ values of 0.616 and 0.605 for MFA and RSA, respectively. The results of the QSAR model were further compared with a structure-based analysis using docking studies with crystal structure of JNK3. Ligands bind in the ATP pocket and the hydrogen bond with GLN155 was found to be crucial for selectivity among other kinases. The results of 3D-QSAR and docking studies validate each other and hence, the combination of both methodologies provides a powerful tool directed to the design of novel and selective JNK3 inhibitors.


The c-Jun N-terminal kinases (JNKs), also called stress-activated protein kinases, are members of the mitogen-activated protein kinase (MAPK) family together with p38 mitogen-activated protein kinases (p38 kinases) and extracellular signal-regulated kinases (ERKs). The JNK MAPK pathway is predominantly activated by stress stimuli and plays important roles in development, apoptosis, cell growth, and immune responses. Three distinct genes encoding JNKs have been identified (jnk1, jnk2, and jnk3), and at least 10 different splicing isoforms are believed to exist in mammalian cells.[1] JNK1 and JNK2 are widely expressed in a variety of tissues. In contrast, JNK3 is selectively expressed in the brain and to a lesser extent in the heart and testis.[1,2]

Experimental instances from knockout studies in mice show that lack in JNK1 or JNK2 results in T-helper (CD4) cell deficiency, while double knockout mice are embryonic lethal. Fibroblasts viable in vitro, however, exhibit a remarkable resistance to radiation-induced apoptosis.[3] JNK3, on the other hand, when deficient, increased resistance to kainic acid-induced apoptosis in the hippocampus. These facts show that JNK activity is crucial in both the immune response and programmed cell death.[4] Therefore, therapeutic inhibition of this enzyme may elicit improvement in clinical treatment of a wide range of apoptosis and inflammatory related diseases such as neurogenerative diseases, ischemia reperfu-

*Keywords*: 3D-QSAR; MFA; RSA; c-Jun N-terminal kinase-3; JNK3 inhibitors; Docking.
* Corresponding authors. Tel./fax: +81 22 795 7235; e-mail addresses: carlos@aki.che.tohoku.ac.jp; miyamoto@ aki.che.tohoku.ac.jp

0960-894X/$ - see front matter © 2006 Elsevier Ltd. All rights reserved.
doi:10.1016/j.bmcl.2006.06.039

sion injuries, multiple sclerosis, rheumatoid arthritis and also recent evidence supports its relevance application in vascular, metabolic, and oncological diseases.[5–7] Nevertheless, isoform selectivity is critical for the development of safe compounds.

Three isoforms of JNK share more than 90% sequence identity and the ATP pocket is 98% similar. It has been found that the same substrate binds with different affinities, and only small differences in primary sequences are present in the primary sequences of the putative binding site. Therefore, designing selective ATP competitive JNK3 inhibitors is a rather challenging task. Crystal structures of JNK3 have been previously reported.[8] Merck researchers have succeeded in crystallizing JNK3 with various small JNK inhibitors.[9] Recently there were a few reports on development of JNK3 isoform ATP competitive inhibitors.[10–12]

A recent one demonstrates that compounds exhibiting benzothiazol-2-ylacetonitrile pyrimidine as their core inhibit JNK3 kinase activity. The reported experimental study based on structure–activity relationship (SAR) studies of a series of potent JNK3 inhibitors leads to the discovery of selective, potent, and in vivo active compound **41**.[13]

In the present study, we have gone beyond the mentioned studies to include 3D-QSAR analyses on a series of benzothiazol-2-ylacetonitrile derivatives in order to provide key structural features required to design highly selective JNK3 inhibitors. Our study includes molecular field analysis (MFA)[14] combined with receptor surface analysis (RSA)[15,16] 3D-QSAR models for JNK3 inhibitors. Furthermore selected inhibitors were docked in the binding pocket of JNK3 in order to single out the main interactions at the atomic and amino acid level between the inhibitors and receptor.

Hitherto, no other study of this nature can be found in the literature, and the 3D-QSAR models that we have obtained for the first time through the present investigation may contribute to a more robust process of design of JNK3 inhibitors taking into account the several structural characteristics and features predicted by our model.

Design of highly selective inhibitors for enzymes requires a detailed analysis of the conformational properties of both the receptor and the inhibitor or ligand molecule. Combining 3D-QSAR modeling for the ligand results in highly accurate models for prediction of the activity of the ligand and its binding characteristics to the receptor. Here, we have collected data on JNK3 inhibitors and we have carried out the structural analysis using MFA and RSA methodologies as described in the following.

A series of benzothiazol-2ylacetonitrile derivatives reported to have rat JNK3 (rJNK3) inhibitory activities was chosen in this study (Table 1).[13] in vitro rJNK3 kinase activities were converted into the corresponding $pIC_{50}$ values ($-\log IC_{50}$). The $pIC_{50}$ values were set as the dependent variable in the MFA and RSA. The total set of JNK3 inhibitors (44 compounds) was divided into a training set (34 compounds) and a test set (10 compounds) in the approximate ratio of 4:1. In order to diversify the training set and test set, they were generated manually so that structurally diverse molecules possessing activities of wide range were included in both sets. The mean biological activity ($pIC_{50}$) of the chosen training and test set molecules was 6.11 and 6.17, respectively.

Three-dimensional structure building and molecular modeling studies were carried out on *Cerius2* Version 4.7.[17] All the structures were initially minimized by OFF methods using the steepest descent algorithm with a gradient convergence value of 0.001 kcal/mol. Partial atomic charges were calculated using the Gasteiger method.[18] Further geometry optimization of each molecule was carried out with MOPAC 6 package using the semi-empirical AM1 Hamiltonian.[19] Alignment was carried out using the MCSG method. This method looks at molecules as points and lines, and uses the techniques of graph theory to identify patterns. It finds the largest subset of atoms in the shape reference compound that is shared by all the structures in the study table and uses this subset for alignment. A rigid fit of atom pairings was performed to superimpose each structure so that it overlays the shape reference compound. Alignment of structures through pairwise superposition placed all the structures of the study compounds in the same frame of reference as the reference compounds, which in our study was the active compound **41**. Even though compound **41** used for the alignment is not the most active, its in vivo efficacy was demonstrated in an experimental model of rheumatoid arthritis.

*Molecular field analysis:* MFA studies were performed using the QSAR module of *Cerius2*.[14,17] The molecular field was created using proton and methyl groups as probes, which represent electrostatic and steric fields, respectively. These fields were sampled at each point of a regularly spaced grid of 1 Å. An energy cutoff of ±30.0 kcal/mol was set for both steric and the total grid points generated were 1260. In addition, the number of spatial and structural descriptors such as dipole moment, polarizability, radius of gyration, number of rotatable bonds, molecular volume, principal moment of intertia, AlogP98, number of hydrogen bond donors and acceptors, and molar refractivity were also considered. Only 10% of the total descriptors for which the variance was the highest were considered for further analysis. Regression analysis was carried out using the genetic partial least squares (G/PLS) method consisting of 50,000 generations with a population size of 100. The optimum number of components was set to 5. Cross-validation was performed with the leave-one-out procedure. PLS analysis was scaled, with all variables normalized to a variance of 1.0.

*Receptor surface analysis:* The same set of aligned molecules was considered for the generation of a receptor surface, using the *van der Waals field function*. The contribution of each molecule for generation of the receptor surface was set to be proportional to its biological

**Table 1.** Structures of JNK3 inhibitors used in this study

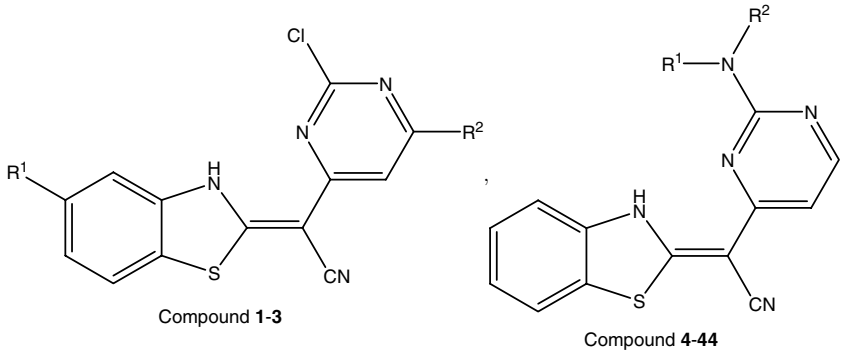


| Compound | $R^1$ | $R^2$ | rJNK3 $IC_{50}$ (nM) |
|---|---|---|---|
| **1** | H | Br | 350 |
| **2** | H | H | 250 |
| **3** | $CF_3$ | H | 993 |
| **4** | H | H | 7500 |
| **5** | H | $NH_2$ | 500 |
| **6** | H | Me | 950 |
| **7** | Me | Me | 9400 |
| **8** | | Piperazinyl | 6600 |
| **9** | | 4-Me-piperazinyl | 6800 |
| **10** | | Morpholinyl | 2900 |
| **11** | | 4-OH-piperidinyl | 7200 |
| **12** | H | $(CH_2)_2N(Me)_2$ | 1300 |
| **13** | H | $(CH_2)_2NH_2$ | 1490 |
| **14** | H | $(CH_2)_2OMe$ | 820 |
| **15** | H | $(CH_2)_2OH$ | 510 |
| **16** | H | $(CH_2)_2N$-piperidinyl | 3740 |
| **17** | H | $(CH_2)_2N$-morpholinyl | 760 |
| **18** | H | $(CH_2)_3N(Me)_2$ | 1644 |
| **19** | H | $(CH_2)_3NH_2$ | 707 |
| **20** | H | $(CH_2)_3OH$ | 660 |
| **21** | H | $(CH_2)_3N$-morpholinyl | 407 |
| **22** | H | $(CH_2)_3N$-(4-Me-piperazinyl) | 473 |
| **23** | H | $(CH_2)_3N$-pyrolidinyl-2-one | 1340 |
| **24** | Me | $(CH_2)_3NHMe$ | 1324 |
| **25** | H | $CH_2Ph$ | 6500 |
| **26** | H | $CH_2$-pyridin-2-yl | 650 |
| **27** | H | $CH_2$-pyridin-3yl | 337 |
| **28** | H | $CH_2$-pyridin-4yl | 340 |
| **29** | H | $(CH_2)_2$-Ph-2-F | 273 |
| **30** | H | $(CH_2)_2$-Ph-3-F | 1810 |
| **31** | H | $(CH_2)_2$-Ph-4-OH | 3500 |
| **32** | H | $(CH_2)_2$-Ph-4-OMe | 3080 |
| **33** | H | $(CH_2)_2$-Ph-4-$NH_2$ | 80 |
| **34** | H | $(CH_2)_2$-Ph-4-$SO_2NH_2$ | 41 |
| **35** | H | $(CH_2)_2$-Ph-4-$NO_2$ | 600 |
| **36** | H | $(CH_2)_2$-indolyl | 458 |
| **37** | H | $(CH_2)_2$-imidazol-4-yl | 80 |
| **38** | H | $(CH_2)_2$-imidazol-4N-Me | 65 |
| **39** | H | $(CH_2)_2$-imidazol-2N-Me | 143 |
| **40** | H | $(CH_2)_2$-pyridin-2-yl | 250 |
| **41** | H | $(CH_2)_2$-pyridin-3-yl | 120 |
| **42** | H | $(CH_2)_2$-*N*-1,2,4-triazolyl | 397 |
| **43** | H | $(CH_2)_3$-*N*-imidazolyl | 147 |
| **44** | H | $(CH_2)_3$-*N*-pyrazolyl | 583 |

activity. The most active compounds **33**, **34**, **37**, **38**, and **41** were used to develop the Receptor Surface Model (RSM). Various chemical properties namely charge, electrostatic potential, hydrogen bonding propensity, and hydrophobicity associated with each surface point were calculated. The interaction energy and strain energy between the molecule and receptor were evaluated and added to the study table. Moreover, the interaction energies of each molecule with methyl (steric) and proton positioned along the grid points throughout the receptor surface were also added to the study table. Only 10% of the total descriptors for which the variance was

the highest were considered independent data to perform further analysis. Regression analysis was carried out using the G/PLS method as described earlier.

Docking studies for selected compounds were carried out using LigandFit[20–22] module of *Cerius2*. The crystal structure of JNK3 (PDB ID: 1PMV)[9] was used for docking studies. The active site was defined as a sphere of radius 6.5 Å surrounding the bound ligand (SP600125). Energetically the most favorable conformation of the docked structure was selected on the basis of the LigandFit score and visual inspection. Initially hydrogen atoms were added to the protein, considering all the residues at their neutral form. Minimizations were carried out using the AMBER force field in Maestro.[23] Minimized structures of docked ligands were submitted for molecular dynamics studies. MD studies were carried out to observe any particular movement of amino acids in the binding site and to get stable ligand–receptor complex. MD studies were carried out using New-Ryudo program developed in our laboratory for 200 ps with step size of 1.0 fs.

Molecular field analysis and RSA 3D-QSAR models were derived using series of benzothiazol-2-yl-acetonitrile derivatives possessing JNK3 inhibitory activities.[13] The training set consisted of 34 compounds while the model was validated using an external set of 10 compounds. The statistical details of the 3D QSAR models are shown in Table 2. Tables 3 and 4 show the actual and predicted activities obtained from MFA and RSA 3D-QSAR models for the training and the test set molecules. Figure 1 shows the graph of actual versus predicted $pIC_{50}$ values of the training set and the test set molecules for MFA and RSA 3D-QSAR models.

The cross-validated $r^2_{cv}$ for MFA model was 0.616, while the non-cross-validated $r^2$ with five components was 0.849. The boot strapping $r^2_{bs}$ value was 0.818. The actual and predicted $pIC_{50}$ values of the training set are shown in Table 3. The $CH_3$ probe represents steric and $H^+$ represents electrostatic descriptors in the QSAR equation of MFA (1). It specifies the regions where variations in the structural features (steric or electrostatic) of the different compounds in the training set lead to increased or decreased activities. The electrostatic descriptor $H^+$ with positive coefficient indicates a region favorable for electropositive group, while negative coefficient indicates electronegative (electron-withdrawing) group required at the position. The MFA model for the activity in terms of the most relevant descriptors is expressed as:

**Table 2.** Statistical details for MFA and RSA 3D-QSAR models

| | MFA | RSA |
|---|---|---|
| $r^2_{cv}$ [a] | 0.616 | 0.605 |
| $r^2$ [b] | 0.849 | 0.766 |
| N[c] | 5 | 5 |
| $r^2_{bs}$ [d] | 0.818 | 0.681 |
| LSE[e] | 0.067 | 0.085 |
| $r^2_{pred}$ [f] | 0.721 | 0.535 |

[a] Cross-validated $r^2$.
[b] Conventional $r^2$.
[c] Number of components.
[d] Bootstrap $r^2$.
[e] Least square error.
[f] Predictive $r^2$.

**Table 3.** Actual and predicted activities of the training set molecules by the MFA and RSA models

| Compound | Actual $pIC_{50}$ | Predicted $pIC_{50}$ | | | |
|---|---|---|---|---|---|
| | | MFA | Residual | RSA | Residual |
| **1** | 6.46 | 6.35 | 0.11 | 6.40 | 0.06 |
| **2** | 6.60 | 6.71 | −0.11 | 6.62 | −0.02 |
| **4** | 5.12 | 5.51 | −0.39 | 5.84 | −0.72 |
| **5** | 6.30 | 5.76 | 0.55 | 6.11 | 0.19 |
| **6** | 6.02 | 6.12 | −0.10 | 6.03 | 0.00 |
| **8** | 5.18 | 5.33 | −0.15 | 5.37 | −0.19 |
| **9** | 5.17 | 5.13 | 0.04 | 4.99 | 0.18 |
| **10** | 5.54 | 5.51 | 0.03 | 5.39 | 0.15 |
| **11** | 5.14 | 5.09 | 0.05 | 4.91 | 0.23 |
| **12** | 5.89 | 5.90 | −0.01 | 6.16 | −0.27 |
| **14** | 6.09 | 6.07 | 0.01 | 6.37 | −0.28 |
| **15** | 6.31 | 6.44 | −0.13 | 5.75 | 0.56 |
| **16** | 5.43 | 5.28 | 0.15 | 5.71 | −0.28 |
| **17** | 6.12 | 5.94 | 0.18 | 5.80 | 0.33 |
| **19** | 6.15 | 6.30 | −0.14 | 6.01 | 0.14 |
| **20** | 6.18 | 6.09 | 0.09 | 6.42 | −0.24 |
| **21** | 6.39 | 6.31 | 0.08 | 6.04 | 0.35 |
| **22** | 6.33 | 6.26 | 0.07 | 6.34 | −0.01 |
| **23** | 5.87 | 6.15 | −0.27 | 5.94 | −0.07 |
| **24** | 5.88 | 5.89 | −0.01 | 6.17 | −0.29 |
| **25** | 5.19 | 5.16 | 0.03 | 5.54 | −0.35 |
| **27** | 6.47 | 6.54 | −0.07 | 6.14 | 0.33 |
| **29** | 6.56 | 6.06 | 0.51 | 6.25 | 0.31 |
| **30** | 5.74 | 6.02 | −0.28 | 6.01 | −0.27 |
| **31** | 5.46 | 5.97 | −0.51 | 6.05 | −0.60 |
| **32** | 5.51 | 5.92 | −0.41 | 5.69 | −0.18 |
| **33** | 7.10 | 6.69 | 0.40 | 6.66 | 0.44 |
| **35** | 6.22 | 6.03 | 0.19 | 6.34 | −0.12 |
| **37** | 7.10 | 7.31 | −0.21 | 7.29 | −0.20 |
| **38** | 7.19 | 6.93 | 0.26 | 7.18 | 0.00 |
| **39** | 6.84 | 6.58 | 0.26 | 6.64 | 0.20 |
| **40** | 6.60 | 6.45 | 0.15 | 6.15 | 0.45 |
| **41** | 6.92 | 7.02 | −0.10 | 6.78 | 0.14 |
| **43** | 6.83 | 6.95 | −0.12 | 6.79 | 0.04 |

**Table 4.** Actual and predicted activities of test set molecules by MFA and RSA models

| Compound | Actual $pIC_{50}$ | Predicted $pIC_{50}$ | | | |
|---|---|---|---|---|---|
| | | MFA | Residual | RSA | Residual |
| **3** | 6 | 5.74 | 0.26 | 6.35 | −0.35 |
| **7** | 5.03 | 5.09 | −0.06 | 5.19 | −0.16 |
| **13** | 5.83 | 6.21 | −0.38 | 5.87 | −0.04 |
| **18** | 5.78 | 5.82 | −0.04 | 6.23 | −0.45 |
| **26** | 6.19 | 6.3 | −0.11 | 6.45 | −0.26 |
| **28** | 6.47 | 6.39 | 0.08 | 6.44 | 0.03 |
| **34** | 7.39 | 7.09 | 0.3 | 5.63 | 1.76 |
| **36** | 6.34 | 5.87 | 0.47 | 6.65 | −0.31 |
| **42** | 6.4 | 6.9 | −0.5 | 6.83 | −0.43 |
| **44** | 6.23 | 5.91 | 0.32 | 6.51 | −0.28 |

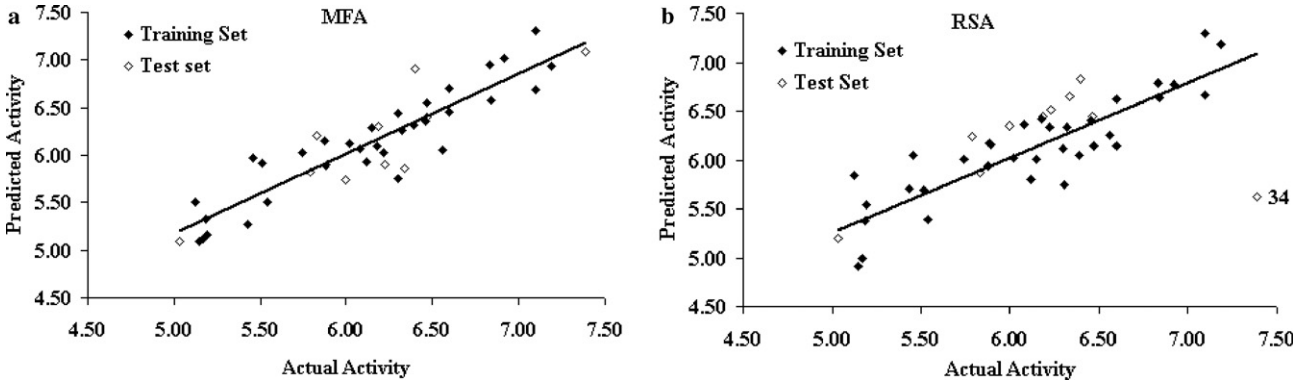


**Figure 1.** Graphs of actual versus predicted $pIC_{50}$ for both training and test set molecules for (a) MFA and (b) RSM 3D-QSAR models (Outlier labeled).

$$\begin{aligned}\text{Activity} = {} & 5.588 + 0.0338 \times (\text{CH3}/208) - 0.0356 \\ & \times (\text{H}^+/147) + 0.0584 \times (\text{H}^+/146) \\ & - 0.0143 \times (\text{CH3}/404) - 0.0237 \\ & \times (\text{CH3}/494) - 0.0122 \times (\text{H}^+/209). \qquad (1)\end{aligned}$$

Presence of two steric descriptors near to *N*-ethyl-3-pyridine group ($CH_3$/404) and ($CH_3$/494) indicates that groups with bigger steric group at these position lead to drop in activity. This can be observed in compounds **18**, **21**, **24**, and **44**. Less activity in compounds **4**–**11** is due to the fact that these molecules are too small and do not completely fit in the binding criteria for steric interactions. As shown in Figure 2, the presence of electrostatic descriptors ($H^+$/147) and ($H^+$/146) near to pyrimidine N indicates the importance of the electrostatic environment at these positions. $H^+$/147 with negative coefficient and $H^+$/146 with positive coefficient indicate that subtle balance of electrostatic parameter is required at these positions. The electron-withdrawing group is necessary at this position. Replacement of pyrimidine N with C atom also leads to drop in activity as found experimentally.[13] The steric descriptor ($CH_3$/208) with positive coefficient indicates that the steric group is favorable at this position. While electrostatic descriptor with negative coefficient ($H^+$/209) indicates that an electron-withdrawing group is required at these positions. Hence, cyanide group can be replaced with a bulkier electron-withdrawing group. When the cyanide group is replaced with ethyl ester a drastic drop in activity is found,[13] these observations indicate that the balance of steric as well as electron-withdrawing groups is crucial for the activity of the compounds.

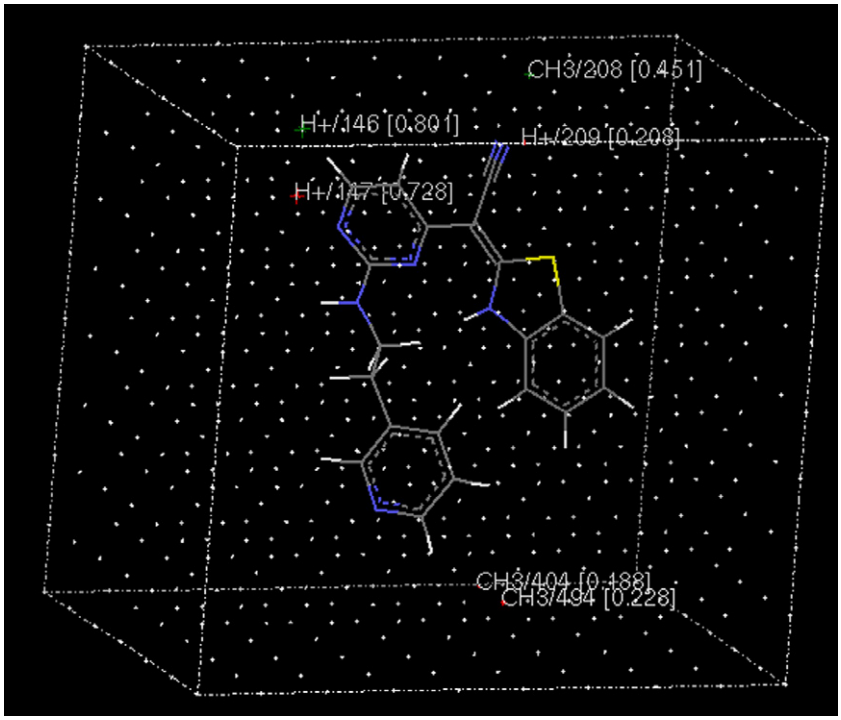


**Figure 2.** Compound **41** within the grid with 3D points of the QSAR equation. $H^+$ represents electrostatic interaction, while $CH_3$ represents steric interaction.

A high $r^2_{cv}$ alone, however, is not a sufficient criterion for a QSAR model to be robust and highly predictive.[24] The predictive power of the model was therefore validated with the test set molecules. The predictive power of the model generated was calculated by Eq. 2:

$$r^2_{pred} = \frac{(SD - PRESS)}{SD}, \quad (2)$$

where SD is the sum of the squared deviations between the biological activities of each molecule and the mean activity of the training set of molecules and PRESS is the sum of squared deviations between the predicted and actual activity values for every molecule in the test set. The prediction of the model was reasonably good with a predictive $r^2$ ($r^2_{pred}$) value of 0.721.

A receptor surface model with $r^2_{cv}$ value of 0.605 and $r^2_{bs}$ value of 0.681 was developed. The conventional $r^2$ was found to be 0.766. The QSAR equation generated by RSM is given in Eq. 3

$$\begin{aligned} \text{Activity} = {} & 6.77147 - 1.48075 \times (\text{ELE}/2640) \\ & - 1.04146 \times (\text{ELE}/1584) - 0.333204 \\ & \times (\text{VDW}/734) + 2.00925 \times (\text{ELE}/397) \\ & - 0.267425 \times (\text{VDW}/2518) - 1.24533 \\ & \times (\text{ELE}/1287) - 0.59127 \\ & \times (\text{ELE}/1168) - 0.7671 \\ & \times (\text{ELE}/2849). \end{aligned} \quad (3)$$

The equation consists of eight molecular field descriptors and their positioning is indicated by the number along with the descriptor. Electrostatic descriptor (ELE/1584) near the benzothiazole –NH group indicates that an electron-donating group is essential at these positions. The electrostatic descriptor (ELE/397) that shows the electrostatic characteristics of the region close to N of pyrimidine ring indicates that an electron-withdrawing group is required for activity at this position. When pyrimidine N is replaced with a carbon atom, the result is an inactive pyridine derivative as found in experimental studies. The electrostatic descriptor (ELE/1168) near to pyrimidine amino N indicates that electron-donating group (N–H) is required at this position. In compounds **7**–**11**, the pyrimidine ring is attached to cyclic amine, while in compound **24** –NH group is replaced with –NMe group, which is responsible for the decrease in activity. This observation indicates that –NH group is very crucial for JNK3 activity. Similarly the steric descriptor (VDW/2518) with negative coefficient near to the pyrimidino amino –NH group evidences that when NH is replaced with any other steric group it will decrease the activity (compounds **7**–**11** and **24**). The electrostatic descriptors (ELE/2640) and (ELE/2849) were found near the tail part of the pyridine ring in compound **41**. Drastic drop in activity for compound **25** is due to the hydrophobic –CH2Ph group that appears at these positions where an electrostatic group is required. In compounds **20**, **21**, **33**, and **34**, electron-donating groups or polar groups are in close vicinity to (ELE/2849) and (ELE/2640) and hence they are moderately active. Similarly compounds **35** and **41** that bear electron-withdrawing groups are also active. These results indicate that electron-donating as well as preferably electron-withdrawing groups in the tail part are essential for activity.

When the charge is mapped on the receptor surface model, it shows a positive contour (blue color) near the S group of the benzothiazole ring (Fig. 3). This indicates that a hydrophobic group is essential at this position and S fulfills this criterion. This observation is consistent with SAR studies where S replaced with a –NH group made the compound inactive.[13] Similarly a negative charge is shown near the tail of the pyridine ring and 1,3 pyrimidine ring on compound **41**. This indicates that an electron-withdrawing group is essential at this position. A red color contour is observed near to pyrimidine ring N and NH group that is attached to pyrimidine indicating the importance of electronegative environment at these positions. Weak intramolecular hydrogen bonding was seen between the N of pyrimidine ring, which acts as an acceptor and the –NH of the benzothiazole ring, which acts as a donor. Hydrogen bonding properties were mapped on the receptor surface as shown in Figure 4. Hydrogen bond donor capability is shown in purple, while cyan color shows hydrogen bond acceptor properties. The cyan color was seen in close proximity of the cyanide (–CN) group, pyrimidine N, and also near to tail pyridine N indicating that hydrogen bond acceptor groups are quite essential at these positions. Benzothiazole –NH and amino group attached to pyrimidine (–HN) is surrounded by cyan color, indicating that electron donor groups are crucial at these positions. The reduced activity of compounds **7**–**11** is due to the fact that there is no hydrogen bond

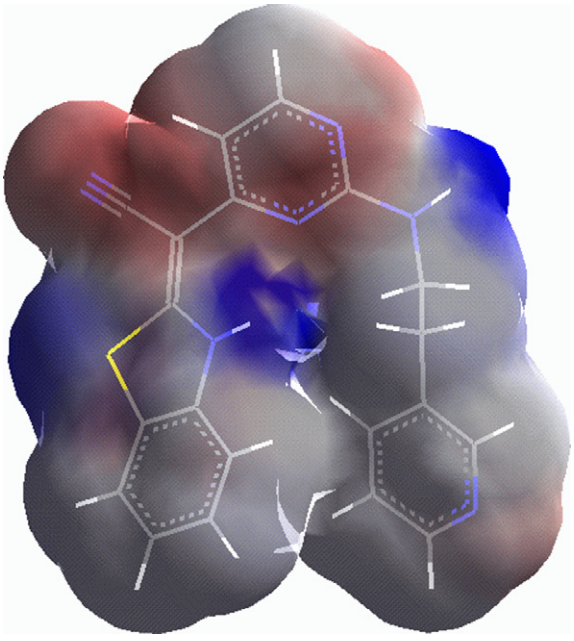

**Figure 3.** Model of the receptor surface on which charges are mapped. Positive regions are shown in blue and negative regions are shown in red. Compound **41** is placed within the generated receptor surface.

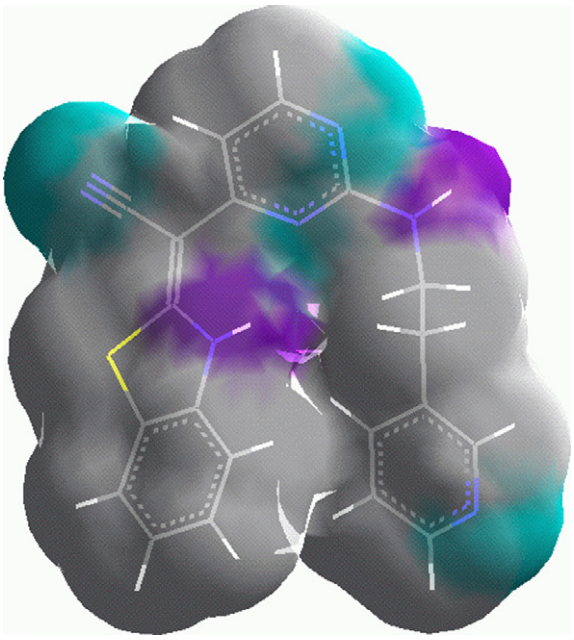

**Figure 4.** Receptor surface model with hydrogen bonding propensity mapped on it. Hydrogen bond donor regions are shown in purple, while hydrogen bond acceptor regions are shown in cyan color. Compound **41** is placed within the generated receptor surface.

donor since the N belonging to a cyclic amino group was used while in compound **24**, –NH group is replaced with –NMe group. As shown in Figure 5, brown color indicates the hydrophobic area, while white color indicates hydrophilic area. The hydrophilic region near to benzothiazole –NH, pyrimidine N, and pyrimidine NH indicates the importance of these groups at these positions.

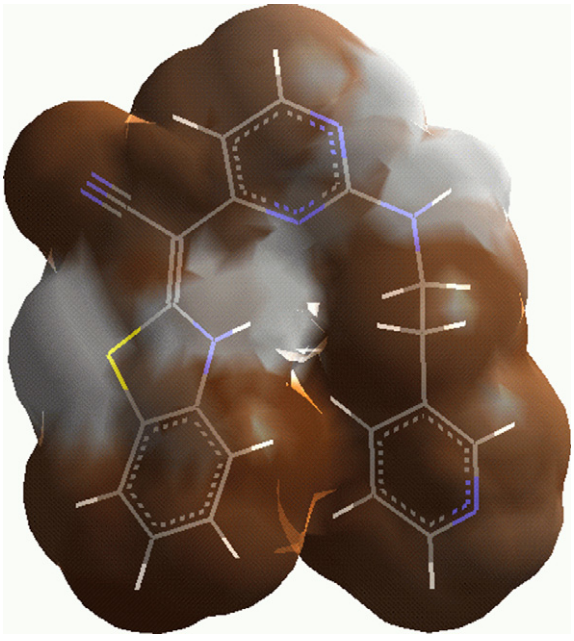

**Figure 5.** Receptor surface model with hydrophobic regions mapped on it. Hydrophobic regions are shown in brown and hydrophilic regions are shown in white. Compound **41** is placed within the generated receptor surface.

Compound **34** was found to be an outlier in the RSM. Its activity is underpredicted. This might be due to the presence of $-SO_2NH_2$ group on the 4th position of the tail part of the phenyl ring. As there were no other compounds with such groups at the 4th position in the training set, the prediction might be wrong. The predictive $r^2$ ($r^2_{pred}$) value was found to be 0.535 without compound **34**. Hence, the predictive ability of RSM model is also high except for compound **34**.

$r^2_{cv}$ for MFA is 0.616 and RSM is 0.605. $r^2_{pred}$ values for both models are listed in Table 2. Statistical analysis for both MFA and RSA 3D-QSAR models indicates that MFA is somewhat better than RSA. In both models, the predictive values fall close to the actual $pIC_{50}$ values, not deviating more than 1 logarithmic unit (Fig. 1, Tables 3 and 4), except for one of the test set molecules (compound **34**) in RSM. Compound **34** is outlier in case of RSM, whereas in MFA, the residual value is 0.3. $r^2_{pred}$ value for MFA is 0.721, while for RSM it is 0.521. Overall both models have good predictive ability while MFA predicted well as compared to RSM.

The structure of the docked compound **41** is shown in Figure 6. Ligand binds in an ATP-binding pocket and hence they can be deemed ATP competitors. Benzothiazole ring binds in a pocket formed by residues Gly71, Ser72, Ser193, Val78, Leu206, Val196, Leu148, and Met149. The docked conformation of compound **41** also shows weak intramolecular hydrogen bond between benzothiazole –NH group and pyrimidine N atom. Acetonitrile group binds in a pocket formed by residues Leu206, Lys93, and Gln75. N in pyrimidine ring forms a hydrogen bond NH group of the backbone of Met149 (N···H–N, 2.26 Å). Similarly Met149 backbone carbonyl group forms a hydrogen bond with the amino group attached to the pyrimidine ring (NH···O=C, 2.03 Å). Hence it mimics the bidentate interaction in ATP molecule and it has been shown in kinases in general to be essential for inhibitor binding.[25,26] The linker *N*-ethyl chain in compound **41** binds with residues: Ile70, Asn152, and Gly71. The tail part of the ligand is the pyridine ring in case of compound **41**. N of pyridine ring forms hydrogen bond with the sidechain of Gln155 (N···HN, 2.26 Å). Gln155 is not conserved in other map kinases and hence it may be at the core of the selectivity for JNKs, which may depend on these types of non-conserved amino acids. Amino acids present in binding site like Lys68, Met146, Asn152, Gln155, and Val196 are non-conserved in p38 and ERK2 kinase, while they are conserved in JNK1, JNK2, and JNK3. Hence selectivity can be achieved against p38 and ERK2 kinase by considering interactions with non-conserved amino acids. This indicates that most of the active compounds under study are selective against other map kinases such as p38, ERK2, and cAMP kinases. Isoform selectivity in JNKs is one of the major challenges in designing selective JNK3 inhibitors. Alignment of JNK3 sequence with JNK1 and JNK2 sequence indicates that residues that come in putative substrate binding domain (Ile246-Tyr268) display the greatest diversity among JNKs isoform. So designing of bidentate inhibitors that extend from the ATP-binding pocket toward

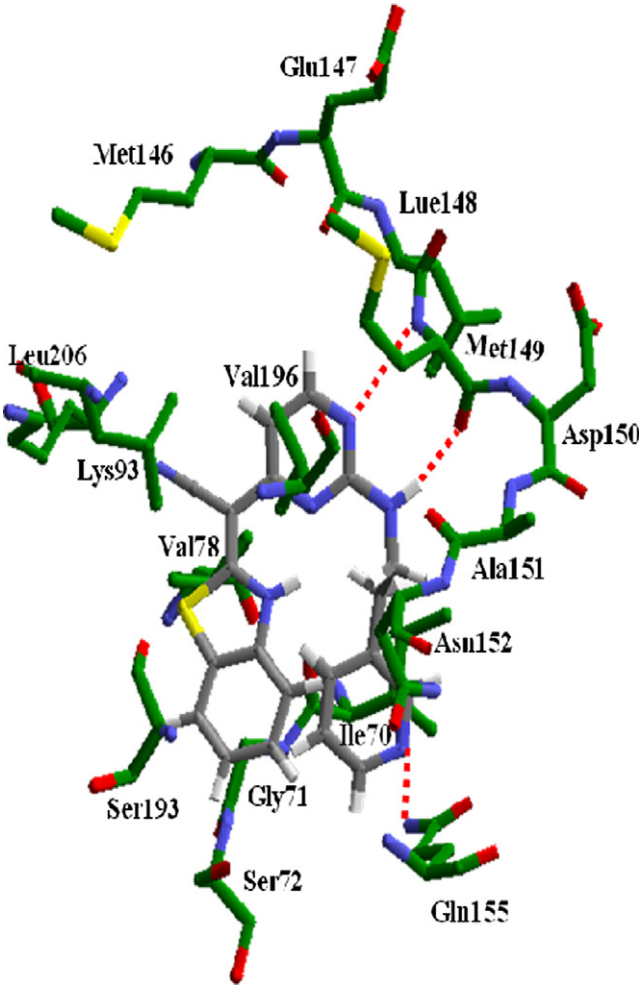


**Figure 6.** Docked conformation of compound **41** (gray) in the binding site of JNK3. All the hydrogen atoms of the protein are removed for clarity. Hydrogen bonds are shown with dotted red lines.

substrate binding pocket may enable us to design selective JNK3 inhibitors. Hence isoform selectivity can be addressed by considering these issues.[9]

Figure 7 shows the superposition of the least active compounds **7** and **9**. The least active compound **7** binds differently as compared to compound **41**. It is almost flipped in the active site (Fig. 7). As this ligand is small in size, there may be many possibilities it can bind in the active site. Compound **9** binds in a similar manner as compound **41** but the hydrogen bond with Met149 is missing since the pyrimidino amino group (–NH) is replaced with pyrimidine cyclic amino group. The hydrogen bond with Met149 is missing together with pyrimidine amino group (NH) in compound **9**. It seems that this pyrimidine –NH group is essential for hydrogen bonding with Met149 and hence it explains the reduced activity for compounds **7**–**11** and **24**. The most active compound **34** forms hydrogen bond with Met149 and Gln155. Our studies indicate that a group such as carboxylic acid at the tail part of the ligand may also improve the activity of the compound due to favorable hydrogen bonding interaction with Gln155 and Asn152 in the binding site.

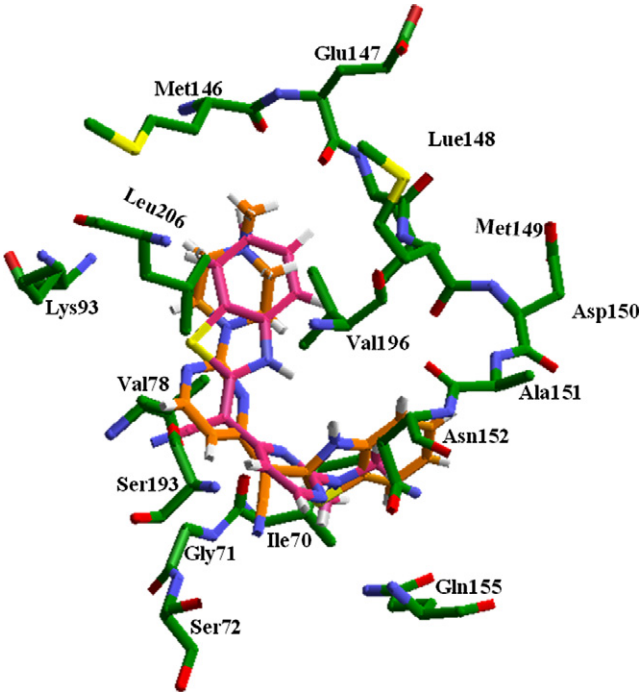


**Figure 7.** Superposition of the docked conformations of compound **7** (pink) and compound **9** (orange) in the binding site of JNK3. Note that compound **7** is flipped in the binding site, while in compound **9** hydrogen bonds with Met149 are missing.

*Comparison between docking and receptor surface analysis:* As shown in Figure 4, the cyan color near to the pyrimidine N indicates hydrogen bond acceptor propensity. Similarly in the docked structure, it has been found that the same pyrimidine N atom forms hydrogen bond with Met149 and hence it act, as hydrogen bond acceptor. Similarly the purple color near to the pyrimidino amino group (–NH) indicates that hydrogen bond donor group is essential at this position, while in the docked structure also a hydrogen bond was found with the backbone of Met149. Both studies indicate that pyrimidino amino (–NH) group is very important for JNK3 activity. And hence it correlates well with RSM model. Similarly, a hydrogen bond was found in between NH group of benzothiazole and pyrimidine N as also shown with RSM model for hydrogen bond propensity (Fig. 4). Tail pyridine ring is surrounded by cyan color indicating hydrogen bond acceptor moiety is required at this particular position. It also correlates well with docking results as pyridine N forms hydrogen bond with Gln155 as shown in Figure 7. The least active compound **7** lacks hydrogen bonding with Met149, which is crucial for inhibitory activity. Similarly this also explains the reason for less activity of compounds **7**–**11** and **24**. Overall docking and 3D-QSAR reveals that two-carbon chain away from amino pyrimidine group is required for selectivity and both acceptor as well as donor group may improve the selectivity since it increases the chances of interaction with Gln155.

In conclusion, 3D-QSAR studies were carried out by building MFA and RSA models. MFA model has better predictive capability than RSA model. Both models yield significant information to build a strategy to

improve the activity of the compounds. The MFA model predicts the importance of proper steric and electrostatic fragments, which are necessary for higher activity. In general pyrimidine ring bearing amino (–NH) group and the linker chain attached to the aromatic hydrogen bond acceptor group are crucial for JNK3 activity. Docking studies revealed that these ligands bind in an ATP-binding pocket. RSA model compared well with docking studies. Hydrogen bonding interaction of the amino pyrimidine ring is crucial for kinase inhibition while selectivity against p38, ERK2, and cAMP can be improved by choosing right structural fragments that can form hydrogen bonds with Gln155. To our knowledge, this is the first study aimed at deriving predictive 3D-QSAR models for JNK3 inhibitors. In addition, the docking studies provided good insights into inhibitor-JNK3 interactions at the molecular level. This information will be very useful in designing novel JNKs inhibitors with broad spectrum of activity against rheumatoid arthritis.

## References and notes


1. Gupta, S.; Barrett, T.; Whitmarsh, A. J.; Cavanagh, J.; Sluss, H. K.; Derijard, B.; Davis, R. J. *EMBO J.* **1996**, *15*, 2760.
2. Mohit, A. A.; Martin, J. H.; Miller, C. A. *Neuron* **1995**, *14*, 67.
3. Yang, D. D.; Kuan, C.-Y.; Whitmarsh, M. R.; Zheng, T. S.; Davis, R. J.; Rakic, P.; Flavell, R. A. *Nature* **1997**, *389*, 865.
4. Lin, A. *BioEssays* **2003**, *25*, 17.
5. Manning, A. M.; Davis, R. J. *Nat. Rev. Drug Disc.* **2003**, *2*, 554.
6. Resnick, L.; Fennell, M. *Drug Discovery Today* **2004**, *9*, 932.
7. Bennett, B. L.; Satoh, Y.; Lewis, A. J. *Curr. Opin. Pharmacol.* **2003**, *3*, 420.
8. Xie, X.; Gu, Y.; Fox, T.; Coll, J. T.; Fleming, M. A.; Markland, W.; Caron, P. R.; Wilson, K. P.; Su, M. S.-S. *Structure* **1998**, *6*, 983.
9. Scapin, G.; Patel, S. B.; Lisnock, J.; Becker, J. W.; LoGrasso, P. V. *Chem. Biol.* **2003**, *10*, 705.
10. Ruckle, T.; Biamonte, M.; Grippi-Vallotton, T.; Arkinstall, S.; Cambet, Y.; Camps, M.; Chabert, C.; Church, D. J.; Halazy, S.; Jiang, X.; Martinou, I.; Nichols, A.; Sauer, W.; Gotteland, J.-P. *J. Med. Chem.* **2004**, *47*, 6921.
11. Heo, Y.-S.; Kim, S.-K.; Seo, C. I.; Kim, Y. K.; Sung, B.-J.; Lee, H. S.; Lee, J. I.; Park, S.-Y.; Kim, J. H.; Hwang, K. Y.; Hyun, Y.-L.; Jeon, Y. H.; Ro, S.; Cho, J. M.; Lee, T. G.; Yang, C.-H. *EMBO J.* **2004**, *23*, 2185.
12. Swahn, B.-M.; Huerta, F.; Kallin, E.; Malmstrom, J.; Weigelt, T.; Viklund, J.; Womack, P.; Xue, Y.; Ohberg, L. *Bioorg. Med. Chem. Lett.* **2005**, *15*, 5095.
13. Gaillard, P.; Jeanclaude-Etter, I.; Ardissone, V.; Arkinstall, S.; Cambet, Y.; Camps, M.; Chabert, C.; Church, D.; Cirillo, R.; Gretener, D.; Halazy, S.; Nichols, A.; Szyndralewiez, C.; Vitte, P.-A.; Gotteland, J.-P. *J. Med. Chem.* **2005**, *48*, 4596.
14. Rogers, D.; Hopfinger, A. J. *J. Chem. Inf. Comput. Sci.* **1994**, *34*, 854.
15. Hahn, M. *J. Med. Chem.* **1995**, *38*, 2080.
16. Hahn, M.; Rogers, D. *J. Med. Chem.* **1995**, *38*, 2091.
17. *Cerius*[2] Molecular Modeling Program Package, Accelrys; Scranton Road, San Diego, CA 92121-3752, USA (<http://www.accelrys.com/>).
18. Gasteiger, J.; Marsili, M. *Tetrahedron* **1980**, *36*, 3291.
19. Dewar, M. J. S.; Zoebisch, E. G.; Healy, E. F.; Stewart, J. J. P. *J. Am. Chem. Soc.* **1985**, *107*, 3902.
20. Luty, B. A.; Wasserman, Z. R.; Stouten, P. F. W.; Hodge, C. N.; Zacharias, M.; McCammon, J. A. *J. Comput. Chem.* **1995**, *16*, 454.
21. Pattabiraman, N.; Levitt, M.; Ferrin, T. E.; Langridge, R. *J. Comput. Chem.* **1985**, *6*, 432.
22. Meng, E. C.; Shoichet, B. K.; Kuntz, I. D. *J. Comput. Chem.* **1992**, *13*, 505.
23. Schrodinger (2001) MAESTRO (Schrodinger, Portland, OR).
24. Golbraikh, A.; Tropsha, A. *J. Mol. Graphics Modell.* **2002**, *20*, 269.
25. Toledo, L. M.; Lydon, N. B.; Elbaum, D. *Curr. Med. Chem.* **1999**, *6*, 775.
26. Boehm, J. C.; Adams, J. L. *Expert Opin. Ther. Pat.* **2000**, *10*, 25.